Applied Catalysis B: Environmental 163 (2015) 444–451

Contents lists available at ScienceDirect

Applied Catalysis B: Environmental

journal homepage: www.elsevier.com/locate/apcatb

Sunlight induced formation of surface Bi_2O_{4-x}–Bi_2O_3 nanocomposite during the photocatalytic mineralization of 2-chloro and 2-nitrophenol

Abdul Hameed[a,b], Muhammad Aslam[a], Iqbal M.I. Ismail[a,c], Numan Salah[d], Paolo Fornasiero[e,*]

[a] Center of Excellence in Environmental Studies (CEES), King Abdulaziz University, Jeddah 21589, Kingdom of Saudi Arabia
[b] National Centre for Physics, Quaid-e-Azam University, Islamabad 44000, Pakistan
[c] Chemistry Department, Faculty of Science, King Abdulaziz University, Jeddah 21589, Kingdom of Saudi Arabia
[d] Center of Nanotechnology, King Abdulaziz University, Jeddah 21589, Kingdom of Saudi Arabia
[e] Department of Chemical and Pharmaceutical Sciences, ICCOM-CNR, University of Trieste, 34127 Trieste, Italy

ARTICLE INFO

Article history:
Received 16 June 2014
Received in revised form 4 August 2014
Accepted 19 August 2014
Available online 26 August 2014

Keywords:
Sunlight photocatalysis
2-Nitrophenol degradation
2-Chlorophenol degradation
Bi_2O_3 based photocatalyst

ABSTRACT

The photocatalytic mineralization of 2-chlorophenol (2-CP) and 2-nitrophenol (2-NP) was investigated using α-Bi_2O_3. The experiments were performed both in complete spectrum and in the visible region (420–800 nm) of the sunlight. The materials were fully characterized by means of UV–vis diffuse reflectance spectroscopy (DRS), photoluminescence (PL), Raman spectroscopy, X-ray photoelectron spectroscopy (XPS) and X-ray diffraction (XRD) analysis and field emission scanning electron microscopy (FESEM). α-Bi_2O_3 showed considerably higher activity for the mineralization of 2-nitrophenol and 2-chlorophenol under natural sunlight exposure, however still appreciable activity was observed in the visible region. Formation of surface nanocomposites Bi_2O_{4-x}–Bi_2O_3 was observed under sunlight irradiation due to the presence of UV light. The sunlight exposed Bi_2O_3, i.e. Bi_2O_{4-x}–Bi_2O_3 composite, showed excellent activity for the degradation and mineralization of 2-CP and 2-NP in the visible region of sunlight. A key role of both hydroxyl and superoxide anion radicals was evidenced in the degradation and mineralization processes under sunlight while only hydroxyl radicals were identified as major facilitators under visible light irradiation.

1. Introduction

The capacity of efficiently removing toxic organic pollutants from the environment is certainly a measure of the quality of human life. In particular, there has been a growing concern in the last decades regarding the presence of carcinogenic and mutagenic compounds in domestic and industrial wastewater. These compounds, even at very low concentrations, cause chronic toxicity, endocrine disruption and enhance the resistance of harmful pathogens [1–3]. These pollutants and their secondary intermediates are often marginally biodegradable and sometimes completely inert toward degradation resulting in an inefficient removal of these toxic compounds by the conventional water treatment procedures [4,5].

Oxidation processes based on the generation of highly reactive transient species (i.e. H_2O_2, OH^-, $O_2^{\bullet -}$, O_3) are considered effective for the simultaneous removal of organic pollutants and disinfection of wastewater pathogens [6]. Photocatalysis has been established as an effective and efficient tool for the removal of various toxic pollutants from water in the presence of light and semiconductor powder. In the recent years, the scientific community has been more and more interested in this emerging technology as it can guarantee an efficient and complete mineralization of a large variety of toxic organic pollutants into harmless products. An ideal photocatalyst for water decontamination is a semiconductor that possesses: (i) high photocatalytic activity, (ii) biological and chemical inertness, (iii) stability toward photocorrosion, (iv) good absorption of visible light or in the near UV region, (v) low cost and (vi) large availability [7]. Solid heterogeneous photocatalysts have the intrinsic advantages of ease of recovery and recycling, being readily amenable to continuous processing.

TiO_2, as it fulfills most of these essential requirements, has been widely used in the degradation of organic pollutants in the water

* Corresponding author. Tel.: +39 0405583973; fax: +39 0405583903.
E-mail address: pfornasiero@units.it (P. Fornasiero).

http://dx.doi.org/10.1016/j.apcatb.2014.08.029
0926-3373/

and air [8–17]. The major drawback of TiO_2 is its fast recombination rates and absorption of UV photons (≤380 nm) for band gap excitation [8]. To overcome this limitation, TiO_2 was doped or co-doped with metals and nonmetals were combined with other semiconductors showing improved photocatalytic performances [17–19]. In an alternative approach, new materials were investigated.

Bi_2O_3 based materials are gaining an increase attention as potentially innovative visible light driven photocatalysts for environmental applications. Among the existing polymorphs of Bi_2O_3, α-Bi_2O_3, because of its versatile properties such as high dielectric permittivity, refractive index, marked photoluminescence and photoconductivity, is used in variety of domains like sensor technology, optical coatings and electro-chromic materials [20–22]. It has been emphasized that depending upon the polymorph and the preparation methodology, the band gap of Bi_2O_3 may vary from about 2.0 to 3.96 eV [23]. α-Bi_2O_3 is an efficient photocatalyst due to its relatively smaller band gap, higher oxidation power of the valence band holes and non-toxic properties [24]. The intrinsic polarizability induced by the Bi^{3+} $6s^2$ lone pair of electrons favors the separation of photogenerated electron–hole pairs. The transfer of these charge carriers makes bismuth a good photocatalyst in the visible region [25]. A significant improvement in the photocatalytic activity of α-Bi_2O_3 was observed by composite formation with ZnO and NiO [26–28]. Recently, the photocatalytic activity of TiO_2–Bi_2O_3 has been also explored [29]. Some of us have previously reported, in a short communication, the photon induced formation of Bi_2O_{4-x} at the surface of α-Bi_2O_3 under UV irradiation generated by a powerful 450 W medium pressure mercury vapor lamp with the intense UV content of ~15% [30]. The formation of the nanocomposite significantly altered the photocatalytic activity of α-Bi_2O_3 for the degradation of methylene blue and phenol. The present study aims to explore the possible formation of Bi_2O_{4-x} on the surface of α-Bi_2O_3 under natural sunlight irradiation and its effect on the optical properties and photocatalytic activity toward the mineralization of 2-CP and 2-NP under complete spectrum and visible region of sunlight before and after the induction of Bi_2O_{4-x} phases. The study identified the nature of oxidizing species involved in the photocatalytic degradation pathways.

2. Experimental details

α-Bi_2O_3 was synthesized by the procedure details in our previous communication [30]. In a typical preparation, the appropriate amount of $Bi(NO_3)_3{\cdot}5H_2O$ was dissolved in 15 mL of concentrated HNO_3 and diluted up to 500 mL. The Bi^{3+} solution was hydrolyzed with KOH solution and adjusted the pH at 8. All the process was carried out under vigorous stirring. The hydrolyzed gel was heated at 200 °C for 2 h and the resultant precipitates were washed with deionized water until neutral pH and removal of all K^+ ions. The precipitates were dried at 120 °C in the hot air oven, crushed and calcined at 450 °C. The synthesis was carried out in a polypropylene apparatus to ensure the silicon free α-Bi_2O_3.

The UV–vis diffuse reflectance spectra of the synthesized α-Bi_2O_3 in the dark and after exposure to sunlight for various intervals were recorded by PerkinElmer UV–vis diffuse reflectance spectrophotometer. All the spectra were recorded using integrating sphere assembly in 200–900 nm wavelength range. The bandgap of the pure and Bi_2O_{4-x}–Bi_2O_3 were evaluated by plotting $(F(R) \times h\upsilon)^{1/2}$ versus $h\upsilon$ (photon energy, eV). $F(R)$ values were calculated by applying Kubelka–Munk transformation to the reflectance data. The room temperature photoluminescence (PL) emission spectra were recorded at an excitation wavelength of 325 nm using a fluorescence spectrofluorophotometer, RF-5301 PC, Shimadzu, Japan. Raman shifts were measured using a DXR Raman Microscope, Thermo Scientific, USA, using a 532 nm laser as the excitation source at 6 mW power.

The XPS profiles of as prepared and sunlight exposed Bi_2O_3 powders were recorded by X-ray photoelectron spectrometer (PHI 5000 VersaProbe II, ULVAC-PHI Inc.). The binding energy was varied between 0 eV and 1100 eV. The oxidation states of Bi were evaluated on the basis of the splitting arises in 4d and 4f levels due to spin–orbit coupling. The FESEM (JEOL JSM 6490-A) was used to examine the morphology of synthesized powders.

To study the photocatalytic activity, the optimized amount of 300 mg of α-Bi_2O_3 was suspended in 150 mL of 30 ppm solution of respective phenol derivative (2-CP or 2-NP). The optimization of α-Bi_2O_3 was carried out by exposing 30 ppm 2-CP solution containing the varying amounts of the catalyst ranging from 100 to 1000 mg for 60 min in a glass reactor. A linear increase in the degradation of 2-CP was observed until 300 mg catalyst loading with the loss of linearity afterwards. Prior to sunlight exposure, the catalyst/substrate suspension was kept in the dark for 3 h. A low adsorption ~5% was observed both for 2-NP and 2-CP. Under sunlight exposure, samples were collected after every 30 min in the first 2 h and after 60 min in the final hour for estimating the progress of degradation process. After removing the catalyst by 0.20 μm syringe filter, the samples were analyzed by HPLC, TOC, IC and GC–MS. All the experiments were performed in the sunlight illumination of $1000 \pm 100 \times 10^2$ lx. As per our observation, the photocatalytic degradation process was only dependent on the illumination intensity while no significant variation in the photocatalytic activity was observed with the change in the angle of incidence. However, for optimum comparison, all the experiments were performed during the fixed duration of sunlight. The decrease in the concentration of phenolic substrate and the formation of intermediates was estimated by HPLC, (SPD-20A, Shimadzu Corporation, Japan) equipped with c18 column and UV detector. Total Organic Carbon (TOC) of the samples was measured by TOC-VCPH total carbon analyzer supplied by Shimadzu, Japan. The ions released during the degradation/mineralization process were identified and quantified by ion chromatograph Dionex (ICS-5000 + EG Eluent Generator) supplied by Thermo scientific, USA. The samples drawn after 30 min of sunlight exposure were analyzed by GC–MS (Shimadzu, Japan, Shimadzu-QP2010 Plus) equipped with RtX1 capillary column, for the identification of unknown intermediate formed during the photocatalytic process using helium (99.99%) as carrier. The experiments in the visible region of the sunlight were performed by adopting the same procedure. The wavelengths below 400 nm were blocked by using Pyrex glass filter.

3. Results and discussion

The preparation and characterization of α-Bi_2O_3 used in this study was reported in our previous communication [30]. Here, we focus on its application for the degradation of 2-CP and 2-NP under solar irradiation and under pure visible light.

The percentage degradation of the phenolic substrates is presented in Fig. 1a. The degradation of both the substrates adopted the similar pattern, however, the observed percentage degradation of 2-NP was slightly lower than that of 2-CP. From the plot, in the initial 30 min of exposure, a low degradation (~30% of the initial concentration) was observed for both the substrates. A significant increase in the degradation was noticed when the exposure time exceeded 60 min and the complete removal of both the substrates was accomplished in 180 min. The rate constants "k" for the degradation of both the substrates was evaluated by plotting $\ln C_o/C$ versus the sunlight exposure time. The graphical evaluation of the rate constants is presented in the inset of Fig. 1. Langmuir–Hinshelwood kinetic model for pseudo first order

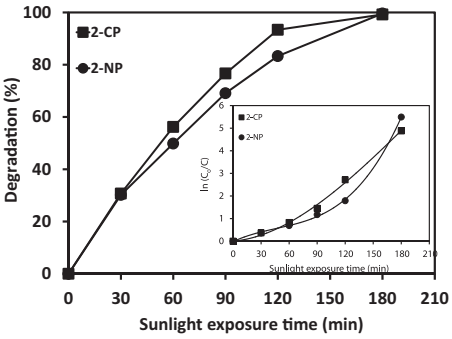

Fig. 1. The comparison of the percentage degradation of 2-CP and 2-NP derived from the decrease in peak height in HPLC profiles. The inset shows the graphical evaluation of the rate of 2-CP and 2-NP degradation over α-Bi_2O_3 (150 mL/300 mg) in sunlight exposure.

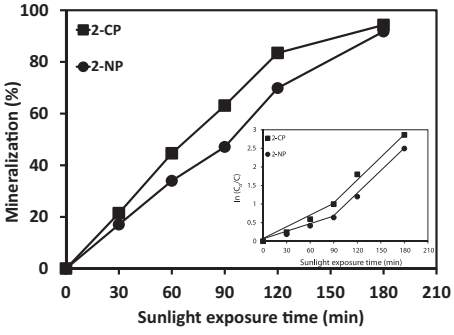

Fig. 2. The comparison of the percentage TOC removal (mineralization) of 2-CP and 2-NP. The inset shows the graphical evaluation of the rate of the TOC removal for 2-CP and 2-NP degradation over α-Bi_2O_3 (150 mL/300 mg) in sunlight exposure.

reactions does not seem to validate the degradation of both the substrates, as after a certain period of time (~90 min) the linearity is lost and an exponential increase in the rates was observed. This observation predicts the change in Bi_2O_3 with sunlight exposure that significantly enhanced the rate of degradation of 2-CP and 2-NP.

It is important to highlight that the HPLC degradation profiles of 2-CP and 2-NP under sunlight show the formation of various intermediates (Supporting information Figure S1). Although qualitatively similar, the behavior is more evident in the case of 2-CP.

The degradation can proceed via two possible pathways: (i) adsorption of 2-CP or 2-NP on the surface of the photocatalyst followed by interaction with photogenerated holes and therefore progressive oxidation or (ii) interaction of the organic molecules in solution with photogenerated radicals. Due to the low/absence of significant adsorption of 2-NP or 2-CP on the surface Bi_2O_3, the main processes after the absorption of photons, are (i) the oxidation of water by the photogenerated holes (h^+) on the Bi_2O_3 that leads to the formation of hydroxyl radicals (Eq. (1)) and/or (ii) the reduction of adsorbed oxygen by photogenerated electrons in the conduction band (e^-) of the semiconductor (Eq. (2)). The formation of hydroxyl radicals requires the suitability of valence band edge for the decomposition of water and favorable conditions of pH [7,8].

$$H_2O + h^+ \rightarrow H_2O^+ \rightarrow HO^\bullet + H^+ \quad (1)$$

$$(O_2)_{adsorbed/dissolved} + e^- \rightarrow O_2^{\bullet -} \quad (2)$$

The reduction of adsorbed oxygen by the photogenerated electrons (Eq. (2)) generates highly oxidizing superoxide anion radicals ($O_2^{\bullet -}$) that are considered the major contributors in the mineralization of organic contaminants [31]. The formation of superoxide anion radicals requires the potential of the conduction band edge higher than −0.28 V. In addition, their lifetime and mobility is pH dependent. At pH lower than the pH_{ZPC}, the existence of superoxide anion radicals is scarce and their conversion to hydroxyl radicals, adopting the following route has been reported [31].

$$O_2^{\bullet -} + H^+ \rightarrow HO_2^\bullet \quad (3)$$

$$HO_2^\bullet + HO_2^\bullet \rightarrow H_2O_2 + {}^1\!/\!_2 O_2 \quad (4)$$

$$H_2O_2 + H^+ + e^- \rightarrow OH^\bullet + H_2O \quad (5)$$

It has been also proposed that at higher pH values, the oxidation of adsorbed hydroxyl anions enhances the formation of hydroxyl radicals [31].

$$HO^- + h^+ \rightarrow HO^\bullet \quad (6)$$

The maximum increase in the concentration of intermediates in the initial 30 min of exposure and a substantial decrease afterwards revealed that the photogenerated oxidizing species, either $O_2^{\bullet -}$ or $HO^\bullet$, initially interact with phenolic substrates. As the concentration of substrates decreases with the increase in the exposure time, the interaction of oxidizing species with the intermediates is initiated and the further degradation of substrates and intermediates proceeds simultaneously.

The time-scale estimation of mineralization process, i.e. removal of total organic carbon (TOC) is presented in Fig. 2. A linear TOC removal can be noticed in the first 90 min of sunlight exposure, after which an exponential increase in the TOC removal was observed. A similar step changed was observed also in the degradation profile of 2-CP and 2-NP (Fig. 1). After 90 min of sunlight irradiation, a ~65% and ~47% TOC removal was measured for 2-CP and 2-NP respectively, which was significantly lower than the degradation (~77% and ~69%) in the same period of time. After only 180 min of irradiation, a TOC removal ≥90% was achieved. The graphical evaluation of the rate constants for TOC removal in the degradation of 2-CP and 2-NP is presented in the inset of Fig. 2. The change rate constant of the mineralization further corroborate previous indications that the absorption of photons can induce changes in α-Bi_2O_3 that enhances the photoactivity.

Bismuth oxide, α-Bi_2O_3, a yellow powder, is a versatile metal oxide semiconductor with a bandgap of 2.8 eV and valance and conduction band edges at +3.13 V and 0.33 V, respectively [32–34]. Being p-type in nature, α-Bi_2O_3 also possesses an excellent electron conduction ability. Based on the potential of conduction band edge, it can be inferred that Bi_2O_3 is unable to reduce the dissolved oxygen that requires −0.28 V for the formation of superoxide anion radicals. However, it has the ability to generate of hydroxyl radicals by adopting the mechanism mentioned in Eq. (1). The identification of the intermediates that appeared in the HPLC chromatograms confirmed the formation of hydroxyl radicals in the degradation of both 2-CP and 2-NP as OH group substituted chloro and nitrophenols were identified in GC–MS analysis along with the presence of aliphatic oxygenates and 2-CP and 2-NP substrates. As mentioned below, the only possible route for the formation of these intermediates is the interaction of hydroxyl radicals with the phenolic substrates.

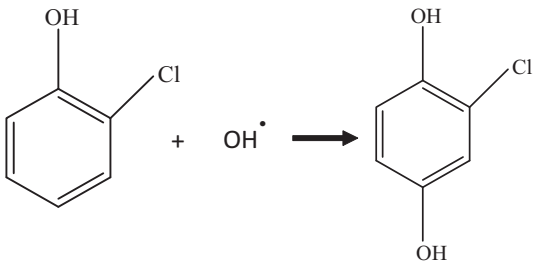

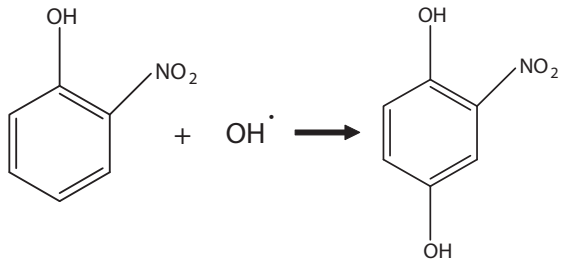

The maximum concentration of these intermediates was observed in the samples analyzed after 30 min of sunlight exposure (Supporting Information Figure S1) and a successive decrease was observed afterwards with increasing exposure time. The multiple substitutions of hydroxyl radicals are also probable; however, no such intermediate was identified.

As presented in Figs. 1 and 2, the initial slow degradation and mineralization of 2-CP and 2-NP substrates with exponential increase afterwards and the identification of aliphatic oxygenates as intermediates predicted the involvement of the superoxide anion radicals both in the degradation and mineralization process. The high mineralization observed is hardly achievable with the interaction of hydroxyl radicals only as it passes through a number of steps while the mineralization by superoxide anion radicals proceeds rapidly.

In our earlier communication [30], we reported the formation of Bi_2O_3–Bi_2O_{4-x} surface composite because of the interaction of highly energetic UV photons with the surface Bi_2O_3 in the presence of dissolved oxygen. The surface Bi_2O_{4-x} imparts brownish appearance to the yellow Bi_2O_3. The comparison of the XRD patterns (Fig. 3) of pure and exposed Bi_2O_3 confirms the formation of nanostructured Bi_2O_{4-x} at the surface of Bi_2O_3. In the XRD pattern of exposed Bi_2O_3, the appearance of reflections at $2\theta = 23.9^\circ$ and $2\theta = 29.5^\circ$ are attributed to oxidized surface Bi_2O_{4-x}.

The comparison of FESEM images of pure and sunlight exposed Bi_2O_3, at different resolutions are presented in Fig. 4a–f, where it can be clearly noticed that only minor surface modifications occur after sunlight exposure while the morphology of the base particles are not affected. EDS analysis confirms the oxidation of part of the Bi that further support the photon generation of surface Bi_2O_{4-x}, highlighted by the arrows in Fig. 4f.

The changes in the optical properties of Bi_2O_3 of the fresh and sunlight-exposed samples, investigated by solid-state absorbance and diffuse reflectance spectroscopy, are fully consistent with the

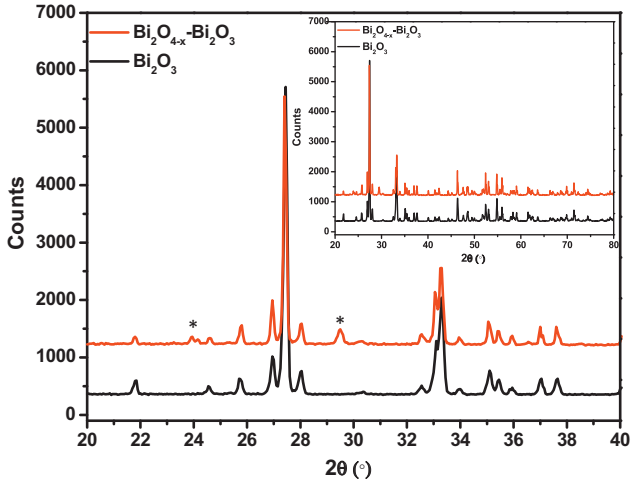

Fig. 3. The comparison of XRD patterns of fresh and exposed Bi_2O_3 from $2\theta = 20^\circ$ to $2\theta = 40^\circ$. The reflection denoted by (*) represent Bi_2O_{4-x}. The inset shows the XRD patterns in 2θ range of 20–80°.

formation of surface Bi_2O_{4-x}. A marked increase in the absorbance in the visible region was observed with time of exposure to sunlight and associated to the progressive formation of Bi_2O_{4-x}–Bi_2O_3 nanocomposite (Fig. 5a). The capability of the brown Bi_2O_{4-x} to increase the light absorption in the visible region of the solar spectrum can be one of the possible reasons of enhanced photocatalytic activity observed upon its formation on the surface of Bi_2O_3. A similar trend was observed in the diffuse reflectance spectra of pure Bi_2O_3 and Bi_2O_{4-x}–Bi_2O_3 (inset of Fig. 5b). A significant decrease in %R was observed for Bi_2O_{4-x}–Bi_2O_3 compared to Bi_2O_3 in the visible region which again depicts the enhanced absorption of visible photons by Bi_2O_{4-x} states. The bandgaps of Bi_2O_3 samples before and after the exposure to sunlight were evaluated by applying Kubelka–Munk transformation on %*R* data. The graphical evaluation of the bandgaps of the powders is presented in Fig. 5b. A bandgap of ~2.7 eV was observed for pure Bi_2O_3, which is in accordance with the literature values [30]. The presence of surface Bi_2O_{4-x} states shifted the bandgap of Bi_2O_3 to slightly lower value of ~2.55 eV which is commonly observable for the composite materials due to matrix effect [30]. The appearance of the additional band edge at ~1.4 eV confirmed the presence of Bi_2O_{4-x} [30]. The appearance of two band edges is consistent with the existence of discrete Bi_2O_{4-x} entities at the surface of Bi_2O_3.

The PL spectra of fresh and exposed Bi_2O_3 are presented in Fig. 6. The emission from unexposed Bi_2O_3 appears in the form of a broad band between 370 to 650 nm. The origin of the maximum intensity peak at ~470 nm (~2.6 eV) is the recombination from Bi^{3+} (6p) to O (2p) and represents the bandgap of Bi_2O_3. An observed significant decrease in the luminescence intensity for the Bi_2O_3 exposed to sunlight for 3 h elaborates the role of photon induced surface Bi_2O_{4-x} in suppressing the recombination process and enhancing the lifetime of the excited states. The decreased luminescence intensity also suggests that these states can induce defects at the surface that serve as a trap for excited electrons.

The comparison of the Raman spectra of as prepared and sunlight exposed Bi_2O_3 is presented in the inset of Fig. 6. The Raman peaks observed were in good agreement with the literature values [35]. The major Raman bands at 528.5, 448.5, 314.4, 211.3 and 152.4 cm^{-1} are attributed to skeletal Bi–O vibrations in as prepared Bi_2O_3. The shifting of these bands to 519.8, 441.7, 309.6, 206.4 and 147.6 cm^{-1} evidences the induction of non-stoichiometry in Bi_2O_3 lattice with the insertion of oxygen. The increased intensity of the all the peaks for sunlight exposed compared to unexposed Bi_2O_3 (inset of Fig. 6) also depicts the measurable changes in the oxygen matrix.

The XPS data (Fig. 7a) of unexposed and sunlight exposed Bi_2O_3 further corroborate the formation of Bi_2O_{4-x} evidencing a change in the relative intensity of the peaks relevant to Bi. In both samples, the Bi4f7, Bi4f5, C1s, Bi4d5 and Bi4d3 peaks appeared at the binding energies of 158.4, 163.8, 284.8, 441.6 and 463.0 eV respectively, which was in accordance with the literature values and confirms the presence of Bi in +3 oxidation states [36,37]. The O1s peak (Fig. 7b) in the as prepared sample appeared at 529.2 eV while that in sunlight exposed Bi_2O_3 at 530.0 eV with increased intensity confirmed the induction of additional oxygen in the lattice.

The sharp increase in the degradation and mineralization ability of Bi_2O_3 after the formation of surface Bi_2O_{4-x} suggests a synergic cooperation between Bi_2O_3 and surface Bi_2O_{4-x} that results in an efficient enhancement of the photocatalytic activity. Bi_2O_{4-x} can serve as "trap" and "transfer" centers for the photogenerated electrons. Additionally, the high mineralization rate in the presence of Bi_2O_{4-x} suggests that they might have also a key role in the formation of superoxide radicals. A pictorial presentation of possible electron trapping and transfer mechanism is presented in Scheme 1.

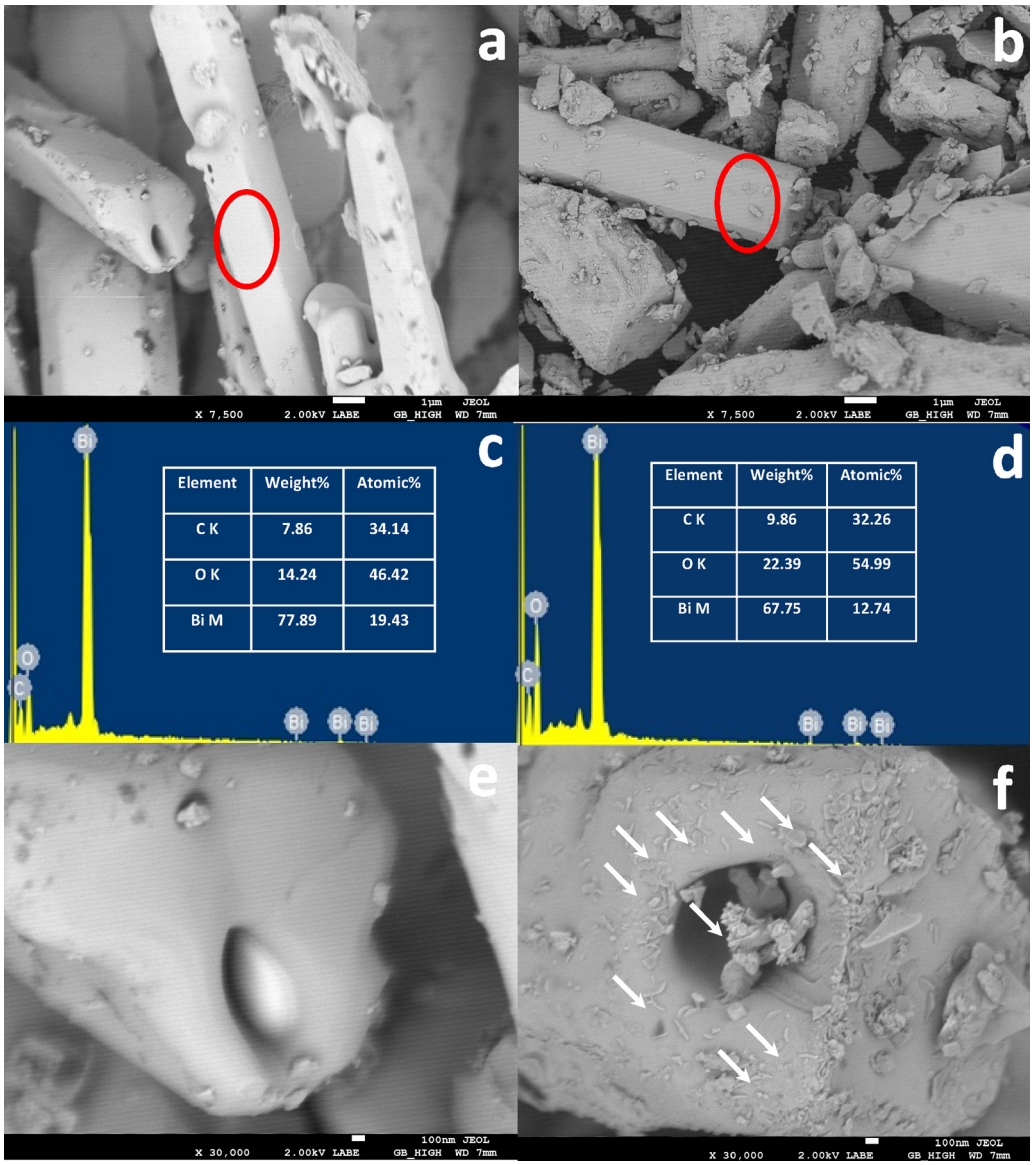

Fig. 4. The FESEM images of unexposed Bi_2O_3 (a and e) and sunlight exposed Bi_2O_3 (b and f) at 7500× (a and b) and 30,000× (e and f) while "c" and "d" shows the EDX spectra of pure and exposed Bi_2O_3. The arrows in "f" indicate the Bi_2O_{4-x} surface states produced after sunlight exposure. The circles (red) in "a" and "b" highlight the areas targeted to acquire EDS spectra. (For interpretation of the references to color in this figure legend, the reader is referred to the web version of the article.)

Since the potential of the conduction band edge of Bi_2O_3 is not appropriate enough to reduce adsorbed/dissolved oxygen, initially the degradation of phenolic substrates is accomplished by the interaction of hydroxyl radicals. The initial slow degradation of 2-CP and 2-NP substrates and the presence of hydroxyl-substituted intermediates predict the same. For extended sunlight exposure times, the formation of surface Bi_2O_{4-x} induces a shifted in the degradation mode from hydroxyl to superoxide anion radicals. The sharp increase in the rate of degradation and mineralization supports this mechanism change.

The mobility and lifetime of the superoxide anions are known [38]. After their generation, the superoxide diffuse in the bulk and interact with the phenolic substrates. Being charged in nature, an entirely different mode of interaction of superoxide anions compared to that of hydroxyl radicals, neutral in nature, can be predicted. Notably that, beside the intermediates formed by the interaction of hydroxyl radicals in the initial 30 min of the sunlight exposure, no aromatic compound or derivative of phenol were identified. Most of the identified compounds were aliphatic intermediates mainly alcohols, carboxylic acids and esters (Scheme 2). The validity of the adopted procedure was judged with the appearance of the original substrates in the GC–MS analysis.

After establishing, that 2-CP and 2-NP are initially transformed into other phenolic derivatives by the interaction of hydroxyl and the formation of Bi_2O_{4-x} promotes the formation of superoxide anion radicals, it was important to estimate the mechanism of interaction of oxidizing radicals (both charged and neutral) with phenolic substrates. The progressive increase of the concentration of chloride ions indicates a direct involvement of charged oxidizing species, and in particular of superoxide anion radicals, both in degradation and mineralization process as the displacement of chloro group of 2-CP as Cl^- by the neutral hydroxyl radicals is not possible. The $O_2^{\bullet-}$ radicals displace the Cl^- ions and the oxygen is incorporated in the carbon chain with ring opening that results in aliphatic oxygenates. The released Cl^- ions further interact with $O_2^{\bullet-}$ to form ClO_2^- ions. The plot of Cl^- and ClO_2^- ions as a function of sunlight exposure time is presented in Fig. 8a. For 2-NP degradation, the release of NO_2^- and the formation of expected ions such

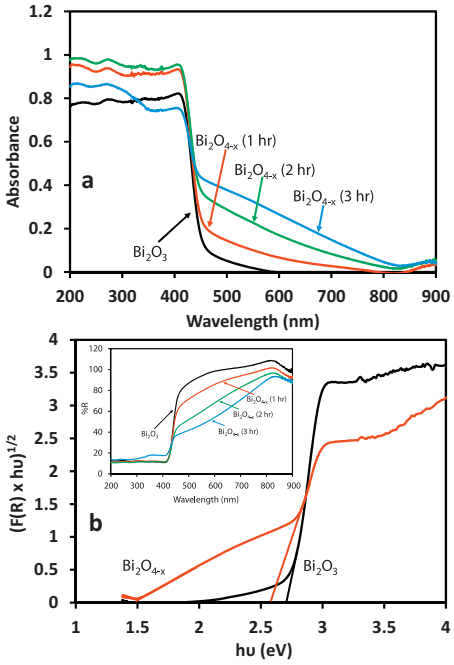

Fig. 5. (a) Comparison of solid-state absorption spectra of pure and Bi_2O_{4-x}–Bi_2O_3 composites formed with various sunlight exposure times and (b) the graphical evaluation of the bandgap of α-Bi_2O_3 and Bi_2O_{4-x}–Bi_2O_3 composite formed after 3 h of exposure. The inset shows the diffuse reflectance spectra of pure and Bi_2O_{4-x}–Bi_2O_3 composites formed at various exposure intervals.

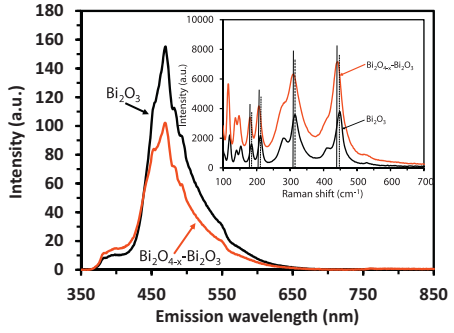

Fig. 6. The photoluminescence spectra (PL) spectra of unexposed (black) and sunlight exposed (red) Bi_2O_3. The inset shows the Raman spectra of unexposed (black) and sunlight exposed (red) Bi_2O_3. The major peaks for unexposed Bi_2O_3 are indicated by dotted lines while for sunlight exposed Bi_2O_3 by solid lines. (For interpretation of the references to color in this figure legend, the reader is referred to the web version of the article.)

as NO_3^- and NH_4^+ ions were also measured (Fig. 8b). In this case a low yield of NH_4^+ ions was observed together with a rapid increase of NO_3^- ions formation after about 90 min of sunlight irradiation. Based on the above mentioned data the mechanism of 2-CP and 2-NP degradation under sunlight irradiation can be illustrated by Scheme 2.

The HPLC profiles for the degradation of 2-CP and 2-NP in the exposure of visible region (≥420 nm) are presented in Supporting Information Figure S2. In comparison to the exposure to complete spectrum sunlight, a significant decrease in the photocatalytic activity for the degradation of both the substrates was observed. The quantity and quality of the intermediates formed was also different in both the cases. Additionally, the formation of hydroxylated aromatic intermediates in appreciable concentration confirmed the formation of hydroxyl radicals during irradiation with pure visible light. These observations further augmented the views that the formation of Bi_2O_{4-x} is induced by UV photons of the sunlight and its

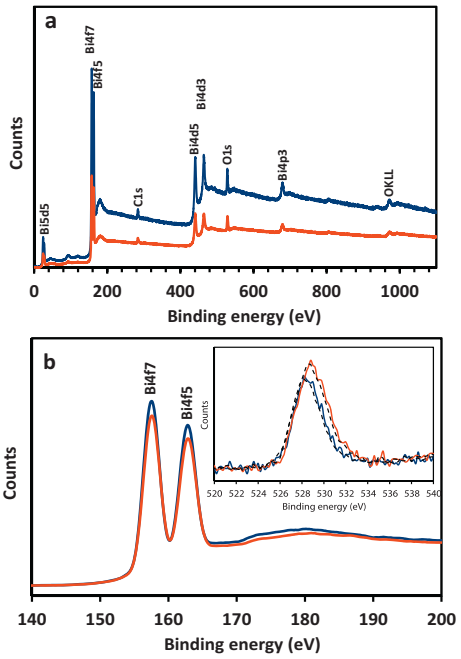

Fig. 7. (a) The comparison of the XPS survey profiles of unexposed (blue) and sunlight exposed (red) Bi_2O_3. (b) The comparison of Bi 4f splitted levels and inset shows the comparison of O1s levels in pure and exposed Bi_2O_3. (For interpretation of the references to color in this figure legend, the reader is referred to the web version of the article.)

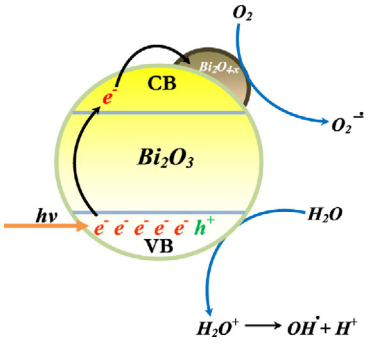

Scheme 1. Possible electron trapping and transfer mechanism in Bi_2O_{4-x}–Bi_2O_3 nanocomposite.

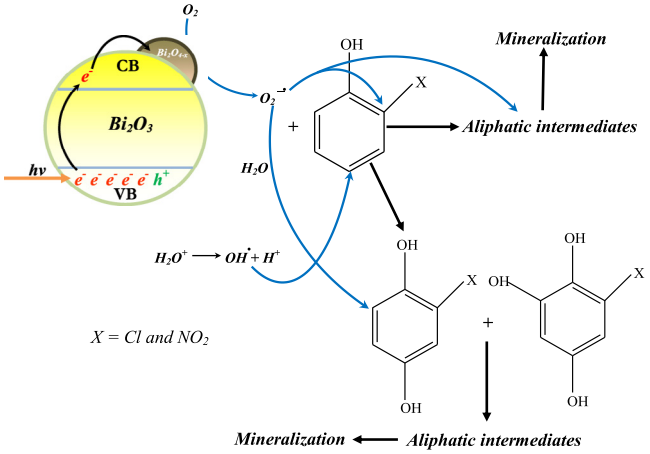

Scheme 2. The mechanism of degradation/mineralization of 2-CP and 2-NP under exposure to the complete spectrum of sunlight.

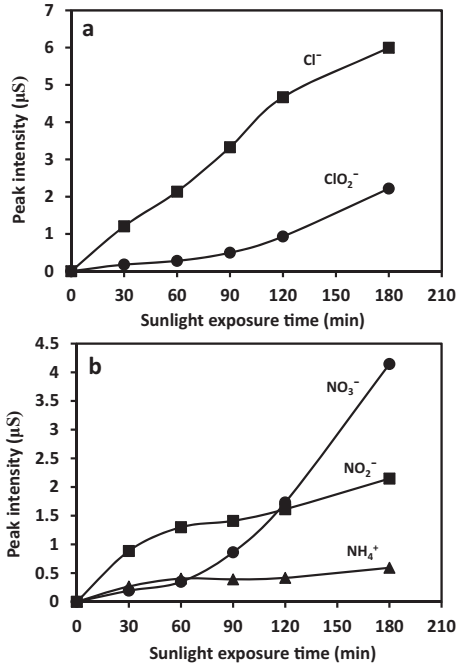

Fig. 8. (a) Release of Cl^- and ClO_2^- ions during the degradation of 2-CP and (b) release of NO_2^-, NO_3^- and NH_4^+ during the degradation of 2-NP over α-Bi_2O_3 (150 mL/300 mg) in sunlight exposure.

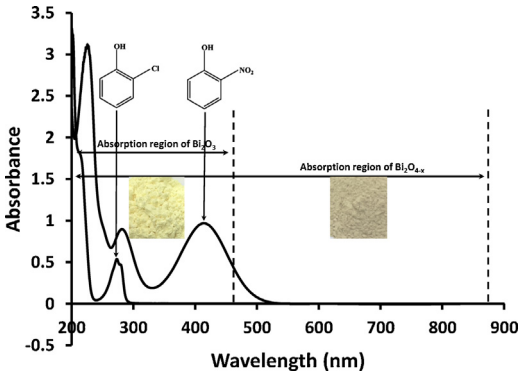

Fig. 9. The absorption spectra of 2-CP and 2-NP adsorbed on Bi_2O_3. Dotted lines identify the absorption regions of Bi_2O_3 and Bi_2O_{4-x}. The inset shows the absorption region of pure Bi_2O_3 (yellow powder) and Bi_2O_{4-x}–Bi_2O_3 nanocomposite (brown powder). (For interpretation of the references to color in this figure legend, the reader is referred to the web version of the article.)

presence facilitates the formation of superoxide anions. The percentage degradation of both the substrate as a function of exposure time in the visible region of sunlight (420–800 nm) is presented in Supporting Information Figure S3a. Compared to >99% degradation of both the substrates during 180 min of the sunlight exposure, ~48% and ~32% of 2-CP and 2-NP were degraded respectively in the pure visible region, corresponding to a decrease photocatalytic activity 60%. More remarkably, at variance to the case of sunlight exposure, no sharp increase in the rates of degradation (Supporting Information Figure S3b) but rather a linear increase following the Langmuir-Hinshelwood kinetic model for pseudo first order reactions was observed. A similar trend was perceived in the removal of TOC. Compared to ≥90% of TOC removal after 180 min of sunlight exposure, ~30% of TOC was removed in the same period under visible light exposure. The low degradation, TOC removal and formation of a variety of the hydroxyl group substituted intermediates predicted that in visible region only hydroxyl radicals contribute to the degradation and TOC removal process. As observed for the catalyst in the complete spectrum of sunlight, no change in the color of the catalyst was observable in 420–800 nm (visible region exposure). This observation led to an important conclusion that only UV photons can induces the formation of Bi_2O_{4-x}. This assumption was further verified by recording the UV–vis DRS spectra of the catalyst exposed to visible region photons for various intervals. The spectra superimposed each other showing no change in the catalyst morphology and formation of Bi_2O_{4-x}.

An intriguing aspect is the significantly low degradation/mineralization of 2-NP compared to 2-CP under visible light irradiation whereas comparable degradation/mineralization rates were found for both the substrates under exposure to the complete spectrum of sunlight. To get insight to this issue, the absorption spectra of 2-NP and 2-CP were recorded after mixing them with the catalyst (Fig. 9). It can be observed that 2-NP possesses a strong absorption band between 400 and 500 nm with λ_{max} = 415 nm. Bi_2O_3 with a bandgap of 2.7 eV (Fig. 5) also requires the absorption of photons in the same region for bandgap excitation and generation of charge carriers. The masking effect of 2-NP in the 400–500 nm range significantly reduces the photon interaction with the catalyst that results in a lower generation of charge carriers that negatively affects the degradation/mineralization process. In the presence of UV photons, such as in the case of the complete sunlight spectrum, the photon adsorption by 2-NP has not a major impact in the final reactivity. In fact, the UV induced formation of Bi_2O_{4-x} leads to an extended spectral response of the catalyst. Vice versa, under pure visible light irradiation, the absence of Bi_2O_{4-x} preclude the formation of superoxide anion radicals significantly affecting the degradation and mineralization rate of 2-NP and 2-CP.

During the degradation of 2-CP, it is observed a substantial decrease in the release of Cl^- ions under pure visible light irradiation compared to the case of complete sunlight irradiation

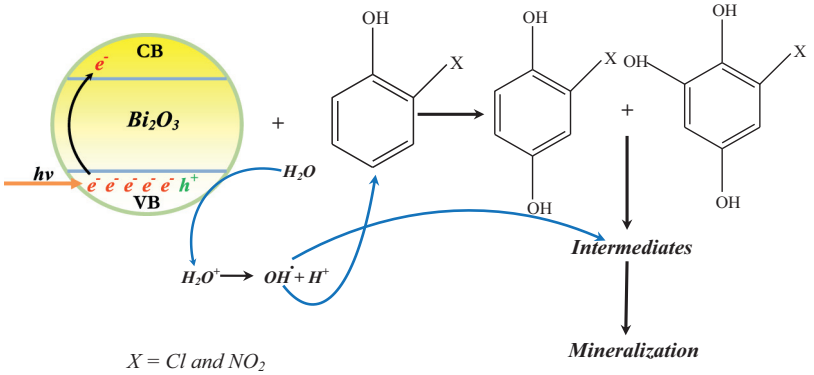

Scheme 3. The proposed mechanism of degradation/mineralization of 2-CP and 2-NP under pure visible light irradiation.

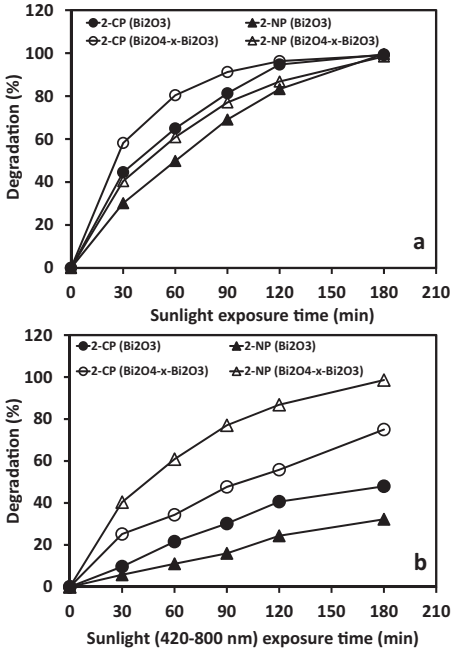

Fig. 10. The comparison of the percentage degradation of 2-CP and 2-NP over fresh and pre-exposed Bi_2O_3 (a) in complete spectrum sunlight exposure and (b) in visible region (420–800 nm) of sunlight.

(Supporting Information Figure S4). The reasons for this decrease have been already discussed. Remarkably, under visible light illumination, no traces of ClO_2^- ions were found suggesting that these ions are formed during 2-CP degradation by the interaction of $O_2^{\bullet-}$ radicals with Cl^- ions. Once more this is consistent with the fact that the formation of $O_2^{\bullet-}$ radicals is unlikely in the absence of Bi_2O_{4-x}, that is generated only by UV irradiations. Notably, the appearance of NO_2^- during the degradation of 2-NP in the visible region of solar spectrum was significantly lower (~negligible) (Supporting Information Figure S4) than that observed under complete sunlight exposure.

Based on all the above-mentioned evidences it can be concluded that the major oxidizing species involved in the degradation of 2-CP and 2-NP under pure visible light irradiation are hydroxyl radicals and follow the mechanism as described in Scheme 3.

Finally, to confirm the key role of Bi_2O_{4-x} in the degradation of 2-CP and 2-NP, it has been investigated the photoactivity of Bi_2O_3, pre-exposed to sunlight for 3 h. Compared to pure Bi_2O_3 a significant enhanced activity was observed for the degradation of phenolic substrates both in the visible region and complete spectrum sunlight (Fig. 10). The HPLC profiles for the degradation of both the substrates are presented in Supporting Information Figures S5 and S6. This observation further strengthen the findings that the surface Bi_2O_{4-x} facilitates the harvesting of incident visible photons and possesses the capability of transferring the photogenerated electrons from the conduction band to the adsorbed oxygen, leading to the generation of superoxide anions. Thus, the presence of pre-formed Bi_2O_{4-x} allows to get a significantly higher activity also under pure visible light irradiation.

4. Conclusions

The present study highlights the importance of the UV portion (≤5%) of sunlight in leading potential structural changes in Bi_2O_3. In particular, the formation of minor concentration of Bi_2O_{4-x} entities not only enhances the spectral response harvesting visible light absorption but also allows the generation of reactive $O_2^{\bullet-}$ radicals. The degradation (loss of aromaticity) and mineralization of 2-CP and 2-NP (resonance stabilized aromatic structures) proves the viability of sunlight as a potential source for photocatalytic studies in future.

Acknowledgments

Authors are greatly indebted to the Center of Excellence in Environmental Studies (CEES), King Abdulaziz University and Ministry of Higher Education (MoHE), Kingdom of Saudi Arabia, for their supports. P.F. acknowledge financial support from the University of Trieste through FRA2013 Project.

Appendix A. Supplementary data

Supplementary data associated with this article can be found, in the online version, at http://dx.doi.org/10.1016/j.apcatb.2014.08.029.

References

[1] C.G. Daughton, T.A. Ternes, Environ. Health Perspect. 107 (1999) 907–938.
[2] T.A. Ternes, A. Joss, H. Siegrist, Environ. Sci. Technol. 38 (2004) 392–399.
[3] P.M. Alvarez, J. Jaramillo, F. Lopez-Pinero, P.K. Plucinski, Appl. Catal. B: Environ. 100 (2010) 338–345.
[4] C. Su, A. Chang, L.M. Bellotindos, M. Lu, Sep. Purif. Technol. 99 (2012) 8–13.
[5] I. Quesada-Penate, C. Julcour-Lebigue, U.J. Jauregui-Haza, A.M. Wilhelm, H. Delmas, J. Hazard. Mater. 221–222 (2012) 131–138.
[6] R. Andreozzi, V. Caprio, A. Insola, R. Marotta, Catal. Today 53 (1999) 51–59.
[7] D.S. Bhatkhande, V.G. Pangarkar, A.A. Beenackers, J. Chem. Technol. Biotechnol. 77 (2001) 102–116.
[8] M.R. Hoffmann, S.T. Martin, W. Choi, D.W. Bahnemann, Chem. Rev. 95 (1995) 69–96.
[9] W. Chao, A. Yan-hui, W. Pei-fang, H. Jun, Q. Jin, Z. Song-he, J. Hazard. Mater. 178 (2010) 517–521.
[10] W. Chao, A. Yan-hui, W. Pei-fang, H. Jun, Q. Jin, Mater. Lett. 64 (2010) 1003–1006.
[11] D.S. Bhatkhande, V.G. Pangarkar, A.A.C.M. Beenackers, J. Chem. Technol. Biotechnol. 77 (2002) 102–116.
[12] C. Lettmann, H. Hinrichs, W.F. Maier, Angew. Chem. Int. Ed. 40 (2001) 3160–3164.
[13] M.A. Lazar, S. Varghese, S.S. Nair, Catalysts 2 (2012) 572–601.
[14] A. Mills, R.H. Davies, D. Worsley, Chem. Soc. Rev. 22 (1993) 417–425.
[15] M.N. Chong, B. Jin, C.W.K. Chow, C. Saint, Water Res. 44 (2010) 2997–3027.
[16] A. Mills, S. Le Hunte, J. Photochem. Photobiol. A 108 (1997) 1–35.
[17] S. Rehman, R. Ullah, A.M. Butt, N.D. Gohar, J. Hazard. Mater. 170 (2009) 560–569.
[18] M. Pelaez, N.T. Nolan, S.C. Pillai, M.K. Seery, P. Falaras, A.G. Kontos, P.S.M. Dunlop, J.W.J. Hamilton, J.A. Byrne, K. O'Shea, M.H. Entezari, D.D. Dionysiou, Appl. Catal. B: Environ. 125 (2012) 331–349.
[19] J. Zhang, Y. Wu, M. Xing, S.A.K. Leghari, S. Sajjad, Energy Environ. Sci. 3 (2010) 715–726.
[20] M. Kositzi, I. Poulios, S. Malato, J. Caceres, A. Campos, Water Res. 38 (2004) 1147–1154.
[21] A.A. Tomchenko, Sens. Actuators B 68 (2000) 48–52.
[22] L. Leontie, M. Caraman, M. Alexe, C. Harnagea, Surf. Sci. 507–510 (2002) 480–485.
[23] L. Leontie, M. Caraman, A. Visinoiu, G.I. Rusu, Thin Solid Films 473 (2005) 230–235.
[24] H. Jiang, K. Cheng, J. Lin, Phys. Chem. Chem. Phys. 14 (2012) 12114–12121.
[25] X. Liu, H. Cao, J. Yin, Nano Res. 4 (2011) 470–482.
[26] A. Hameed, V. Gombac, T. Montini, M. Graziani, P. Fornasiero, Chem. Phys. Lett. 472 (2009) 212–216.
[27] A. Hameed, V. Gombac, T. Montini, L. Felisari, P. Fornasiero, Chem. Phys. Lett. 483 (2009) 254–261.
[28] L. Cheng, Y. Kang, J. Alloys Compd. 585 (2014) 85–93.
[29] J. Chen, S. Qin, Y. Liu, F. Xin, X. Yin, Res. Chem. Intermed. 40 (2014) 637–648.
[30] A. Hameed, T. Montini, V. Gombac, P. Fornasiero, J. Am. Chem. Soc. 130 (2008) 9658–9659.
[31] P. Pichat, Photocatalysis and Water Purification From Fundamentals to Recent Applications, 1st ed., Wiley-VCH Verlag GmBH, Germany, 2013.
[32] P. Maruthamuthu, K. Gurunathan, E. Subramanian, Int. J. Hydrogen Energy 19 (1994) 889–893.
[33] K. Gurunathan, Int. J. Hydrogen Energy 29 (2004) 933–940.
[34] Y. Xu, M.A.A. Schoonen, Am. Mineral. 85 (2000) 543–556.
[35] C.H. Ho, C.H. Chan, Y.S. Huang, L.C. Tien, L.C. Chao, Opt. Express 21 (2013) 11965–11972.
[36] D. Barreca, F. Morazzoni, G.A. Rizzi, R. Scotti, E. Tondello, Phys. Chem. Chem. Phys. 3 (2001) 1743–1749.
[37] Y. Dai, Y. Wang, J. Yao, Q. Wang, L. Liu, W. Chu, G. Wang, Catal. Lett. 123 (2008) 307–316.
[38] T. Hirakawa, Y. Nosaka, Langmuir 18 (2002) 3247–3254.